XLIII CILAMCE
21–25, November, 2022
FOZ DO IGUAÇU – PR – BRAZIL

Fully explicit FEM formulation for NMR simulations using the Dufort-Frankel method

Luiz F. Bez[1], Ricardo Leiderman[1], André Souza[2], Rodrigo B. de V. Azeredo[3], André M. B. Pereira[1]

[1]*Institute of Computing, Universidade Federal Fluminense*
Av. Gal. Milton Tavares de Souza s/n, Niterói, 24210-310, RJ, Brazil
lfbez@id.uff.br, leider@ic.uff.br, andre@ic.uff.br
[2]*Institute of Geosciences, Universidade Federal Fluminense*
R. São João Batista, 2-188, Niterói, 24020-007, RJ, Brazil
aasouza@id.uff.br
[3]*Institute of Chemistry, Universidade Federal Fluminense*
R. São João Batista, 2-188, Niterói, 24020-007, RJ, Brazil
rodrigo.bagueira@gmail.com

Abstract. In this paper we present a fully explicit finite element implementation for the simulation of the T_2 relaxation and T_1 recovery process in nuclear magnetic resonance experiments. We consider 2D domains defined by images. We propose the combination of a lumped mass matrix and stable time-marching schemes to achieve a fully explicit and stable simulation even with large time steps. The time-marching scheme we consider is the Dufort-Frankel method which allows for large time-steps even for problems in the fast diffusion regime. We show that the use of the lumped mass matrix adds a negligible amount of numerical error in comparison to the error introduced by the discretization. We also show that this method compare favorably to the Explicit Euler in terms of necessary number of time steps in order to achieve a reasonable threshold of numerical error.

Keywords: NMR, Petrophysics, Dufort-Frankel

1 Introduction

Nuclear Magnetic Resonance (NMR) is a successful technique applied to petrophysical characterization of porous reservoir rocks [3, 5]. The technique consists in the application of a static magnetic field to polarize the sample's nuclei that possess an angular spin moment and hence a net magnetic moment. This polarization creates a net magnetization from the sum of each nuclei spin, which is then manipulated via the application of a secondary magnetic field applied in the form of a finite pulse. Through the application of a single radio-frequency pulse or a specific designed pulse sequence, the evolution of such polarized spin system reveals relevant aspects of the physical-chemical properties of the sample.

Two of the most common application evolves the spins to probe the so-called T_1 and T_2 relaxation processes, when the return to the equilibrium state of the magnetization depends on the pore-size information and the strength of the fluid/matrix interaction [5]. The T_2 relaxation process measures the loss of signal coherence caused by the bulk, surface and magnetic field heterogeneities interactions. The T_1 process measures the rate of return of the spin coherence towards an equilibrium magnetic field, due to bulk and surface interactions.

The pore space of a given rock can be probed via these processes because the resulting signal is intimately linked to the pore size distribution of the sample, specially in fast diffusion scenarios [3, 5]. These results can be simulated digitally based on X-ray micro-computed tomography (micro-CT) images of rocks at an adequate resolution, if they can well represent its pore space. These micro-CT images are a common resource in digital petrophysics, and, in general, these digital representations can be formed by millions of individual pixels. The use of this resource as a geometric representation for numerical simulations can prove challenging, both due to the size of the problem and its numerical characteristics.

One possible way to simulate this phenomenon is to solve the continuum equation that represents the T_2/T_2 relaxation problem. This equation can be solved numerically via many different methods. The approach that we will focus on here is the one using the Finite Element Method (FEM) to discretize the governing equations. It allows for the simulation of complex domains, with the direct representation of the continuous magnetization

function. It also has greater flexibility to couple the magnetization evolution with extra phenomena - such as internal magnetic field gradients [10] and fluid flow [1],[2].

One major aspect of the FEM simulations of fast diffusion processes is the inherent numerical instability of the process. Traditional explicit methods require a prohibitively small time-step size to be stable. It is possible to tackle this problem with methods of increased stability like Runge-Kutta-Chebyshev (RKC) [9] or even to solve the problem for its eigenfunctions-eigenvalues pairs representing the most important relaxation modes and times [8].

The approach that we have here is to adopt the Dufort-Frankel method, which uses the indirect hyperbolization of the differential equation in order to achieve stability. This method, combined with the use of a lumped-mass matrix system allows for a fully explicit time-integration process with minimal losses due to numerical error. We show the magnitude of the influence of the choice of lumped mass and also in practical terms the reduction in time-step number that can be achieved for a reasonable error threshold.

2 Mathematical and numerical modeling

2.1 Differential problem

Let Ω be the pore space, in the cases considered here a proper open subset of $\mathbb{R}^2$. The pore domain may be formed by a set of disconnected regions or by a single region. Let Γ be the pore interface $\Gamma \equiv \overline{\Omega} \setminus \Omega$. Let $m_{1,2}(\mathbf{r},t) : [\overline{\Omega},\mathbb{R}_{\geq 0}] \rightarrow \mathbb{R}_{\geq 0}$ be the nuclear magnetization intensity - m_1 for the longitudinal recuperation problems and m_2 for the transversal relaxation problems. In the absence of a magnetic field gradient, the reaction-diffusion equation can model the magnetization relaxation response as [11]:

$$\frac{\partial m_2}{\partial t} = D_0 \nabla^2 m_2 - \frac{1}{T_b} m_2 \tag{1}$$

where $D_0 \in \mathbb{R}_{>0}$ is the bulk diffusion coefficient $[\mu m^2/s]$, and $T_b \in \mathbb{R}_{>0}$ is the bulk relaxation time $[s]$. At the pore interface Γ a partially absorbing boundary condition applies as $D_0 \nabla_{\hat{\mathbf{n}}} m_2 + \rho_2 \, m_2 = 0$, where $\hat{\mathbf{n}}$ is the outward normal vector to the boundary, and $\rho \in \mathbb{R}_+$ is the surface relaxivity $[\mu m/s]$. We will consider no relaxation due to magnetic field gradients, and the initial condition will be an uniform magnetization, set at a reference value m_0, *i.e.* $m(\boldsymbol{r},0) = m_0 \; \forall \boldsymbol{r} \in \overline{\Omega}$. In all cases as $t \rightarrow \infty$ the magnetization $m(\boldsymbol{r},t) \rightarrow 0$, as it is expected given the context of the phenomenon we are simulating.

Similarly, the problem of the longitudinal recuperation can be formulated using the diffusion reaction equation with Robin boundary conditions. The main difference is that now the magnetization goes from a starting value m_s to a reference value m_0 as $t \rightarrow \infty$. The differential equation that represent this problem is:

$$\frac{\partial m_1}{\partial t} = D_0 \nabla^2 m_1 - \frac{1}{T_b}(m_1 - m_0) \tag{2}$$

with $D_0 \nabla_{\hat{\boldsymbol{n}}} m_1 + \rho_1 \; (m_1 - m_0) = 0$ as its boundary condition. Since the problem we are analyzing is linear, all the simulations will be performed in a way to evolve the magnetization within a unitary interval. By setting m_0 to 1 and m_s to zero, we will have m_1 and $m_2 \in [0,1]$ - m_1 going from 0 to 1 and m_2 from 1 to 0 as time goes from 0 to ∞. If we consider a unitary step problem instead of a generic one the magnetization referring to T_1 and T_2 problems would be identical apart from a multiplicative factor.

The quantities that will be analyzed will be the magnetization of the whole domain normalized by the initial magnetization in a T_2 simulation or the reference magnetization in a T_1 simulation. They are defined as:

$$M_i(t) = \frac{\int_\Omega m_i(\mathbf{r},t) \, \mathrm{d}\Omega}{\int_\Omega m_0 \, \mathrm{d}\Omega}, \quad i = 1,2 \tag{3}$$

$M(t)$ will be used in every convergence analysis. In the case studies we also analyze the inverse Laplace transform of $M(t)$, which gives us the T_1 and T_2 time distributions. This distributions relate directly to the surface-to-volume ratios of pores in a fast diffusion regime. The inversion problem is usually ill-posed and numerically

unstable. In order to improve the conditions of these inversions, we add a white noise component to $M(t)$, in a signal-to-noise ratio of $2000:1$. Additionally the inversion is performed using Tikhonov regularization, with a regularization factor set at 0.15.

The equations 1 and 2 cannot be solved analytically for any given pore network. In this work we will use the Finite Element Method (FEM) to approximate the spatial derivatives, and a number of explicit time-marching schemes to solve the temporal evolution of the problem.

2.2 Finite element formulation

Consider $w(\boldsymbol{r}) : \mathbb{R}^2 \to \mathbb{R}$ to be a sampling function. The weak formulation for the m_2 problem is given by:

$$\int_\Omega \frac{\partial m_2}{\partial t}\, w \,\mathrm{d}\Omega + \int_\Omega D_0 \nabla m_2 \cdot \nabla w \,\mathrm{d}\Omega + \int_\Omega \frac{1}{T_b} m_2 \, w \,\mathrm{d}\Omega + \int_\Gamma \rho_2 \, m_2 \, w \,\mathrm{d}\Gamma = 0 \tag{4}$$

We will use Galerkin approach, with the shape functions being the same as the sampling functions - in our case, bi-linear interpolating polynomials.

Let $\boldsymbol{m_2} = [m_{2,i}]$ be the vector of the approximate solution at each node i. The last three integrals in Eq. 4 will compose the stiffness matrix $\boldsymbol{K}$, whose elements are defined by:

$$\mathbf{K} = [K_{ij}] = \left[\int_{\Omega_i} D_0 \mathbf{B_i^T B_j} + \frac{1}{T_b} N_i N_j \mathrm{d}\Omega_i + \int_{\Gamma_i} \rho N_i N_j \mathrm{d}\Gamma_i \right] \tag{5}$$

where $\mathbf{B_i}$ is the gradient of N_i, and Ω_i and Γ_i are the compact support domain and boundary correspondent to the i-th node. In a element that is not a part of the pore domain's boundary, the set Γ_i is empty and the last integral in eq. 5 does not contribute to $\mathbf{K}$.

The first integral in Eq. 4 will compose the capacitance matrix. We will study two forms for this matrix in this paper: the so-called consistent capacitance matrix, that has no simplifying hypothesis; and a lumped capacitance matrix, where the contributions are independently calculated node-by-node resulting in a diagonal matrix. Therefore, the former is much more expensive to invert than the latter. Considering $\mathbf{C}$ to be a stand-in for either type of capacitance matrix, the numerical system to be solved is expressed by:

$$\frac{\mathrm{d}}{\mathrm{d}t}\mathbf{m_2} = -\left(\mathbf{C}^{-1}\mathbf{K}\right)\, \mathbf{m_2} \tag{6}$$

In a similar fashion we can write the residual equation for the m_1 problem:

$$\int_\Omega \frac{\partial m_2}{\partial t}\, w \,\mathrm{d}\Omega + \int_\Omega D_0 \nabla m_2 \cdot \nabla w \,\mathrm{d}\Omega + \int_\Omega \frac{1}{T_b} m_2 \, w \,\mathrm{d}\Omega + \int_\Gamma \rho_1 \, m_2 \, w \,\mathrm{d}\Gamma + \\ - \int_\Omega \frac{1}{T_b} m_0 \, w \,\mathrm{d}\Omega - \int_\Gamma \rho_1 \, m_0 \, w \,\mathrm{d}\Gamma = 0 \tag{7}$$

where the two last integrals will compose the body force vector - since they do not involve the unknown m_1 function. The matrices $\boldsymbol{C}$ and $\boldsymbol{K}$ are identical to the ones used in the m_2 problem. The body force and the matrix system are defined as:

$$\mathbf{b} = [b_i] = \left[\int_{\Omega_i} \frac{1}{T_b} N_i \, m_0 \mathrm{d}\Omega_i + \int_{\Gamma_i} \rho \, N_i \, m_0 \mathrm{d}\Gamma_i \right] \tag{8}$$

$$\frac{\mathrm{d}}{\mathrm{d}t}\mathbf{m_1} = -\left(\mathbf{C}^{-1}\mathbf{K}\right)\, \mathbf{m_1} + \boldsymbol{b} \tag{9}$$

2.3 Explicit time-integration

Equations 6 and 9 will be solved using two explicit time-marching algorithms. The first is the simplest and fastest, the Explicit Euler scheme. The second is the Dufort-Frankel scheme.

The Explicit Euler is a first-order time marching scheme, where the derivative in time is replaced by a finite difference, and the right side of eq. 9 is evaluated at the previous time-step. The nodal magnetization at time t is then defined as:

$$\mathbf{m}^t = \mathbf{m}^{t-1} - \Delta t \left(\mathbf{C}^{-1}\mathbf{K}\right) \mathbf{m}^{t-1} + \boldsymbol{b}^{t-1} \tag{10}$$

where Δt is the chosen time step size, and $\mathbf{m}^t$ is a stand-in for the nodal values of either m_1 or m_2 at time t. Our body force vector $\mathbf{b}$ does not vary with time, so $\mathbf{b}^t$ is the same for any t. Notice that this scheme is conditionally stable. This stability is restrictive, especially due to mesh refinements. For a 2D pore domain, we observed that this method requires $\Delta t = \mathcal{O}(1/D_0\,\Delta x^3)$ in order to be stable. In our implementation we set the maximum Δt value to $0.1/D_0\,\Delta x^3$ heuristically.

The Dufort-Frankel is a second-order explicit time-marching method that uses a different treatment for the diagonal terms of $\mathbf{C}$ and $\mathbf{K}$ in order to achieve unconditional stability [4]. The left side of Eqs. 6 and 9 is approximated with a central finite difference scheme, between the steps t and $t-2$, while the right side of eq. 6 is evaluated at time $t-1$. However, the diagonal contribution of these right side terms will be applied to a linear interpolation of time t and $t-2$. The nodal magnetization at time t is then defined as:

$$\mathbf{m}^t = \tilde{\mathbf{C}}^{-1}\left(\mathbf{C} - \Delta t\mathbf{K_d}\right)\mathbf{m}^{t-2} - 2\Delta t\tilde{\mathbf{C}}^{-1}\left(\mathbf{K} - \mathbf{K_d}\right)\mathbf{m}^{t-1} + 2\Delta t\tilde{\mathbf{C}}^{-1}\mathbf{b} \tag{11}$$

where $\tilde{\mathbf{C}} \equiv (\mathbf{C} + \Delta t\mathbf{K_d})$, and $\mathbf{K_d}$ is a diagonal matrix composed by the diagonal elements of $\mathbf{K}$ - notice that if we use a lumped capacitance matrix $\tilde{\mathbf{C}}$ can be inverted trivially. This method can be applied for any time step size. However, for large time-steps $M(t)$ may not converge to the correct limiting value as t goes to infinity. This behavior was analyzed by [6] and was observed in this study.

Since this method requires two time-step solutions in each iteration, we choose to solve the first step using the Modified Euler method in order to keep the second order convergence. This method will have the same stability threshold as the Explicit Euler, and therefore a number of sub-steps may be needed to correctly initialize the solution.

3 Numerical results

In this section we will present convergence and validation studies. In a first moment we will use a 1D gap model to test the influence of the diagonalization of the mass matrix and successive mesh refinements. In the next subsection we will use an artificial arrangement of circular pores to test convergence and accuracy of the method for a fast diffusion problem.

Numerical convergence analysis were performed by measuring the deviation ε of the average magnetization between two simulations, in infinity norm. Each time, one discretization parameter is changed (i.e. mesh, time-step size, or type of capacitance matrix) while the remainder are held constant.

3.1 One dimensional gap model

This simple model, described in the figure below, is used to investigate the influence of the type of capacitance matrix and the influence of successive mesh refinements. The process of time integration with the consistent matrix demands the solution of a linear system in each step of the simulation, therefore being very expensive. This simple model, being able to be well represented by a minimal mesh, is useful to perform this kind of comparison.

Four parameter sets and were considered: $\{(D_0/\rho L, T_b)_i\} = \{(100,0.1),(100,\infty),(10,\infty),(1,\infty)\}$. All of them are considered with time going from zero to one second, length $L = 1\mu m$, $\rho = 10\mu m/s$, and homogeneous unitary initial condition for the T_2 relaxation problem. In the comparisons shown in this section, the T_1 problem present equivalent behavior both qualitatively and quantitatively. Five different mesh sizes were consider, for all parameter sets, with the number of divisions N_x going from 2 to 32 divisions in L.

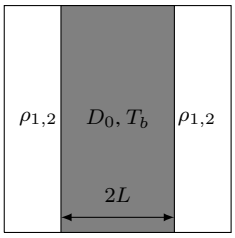

Figure 1. One dimensional gap model.

Table 1. Numerical deviation with matrix type and mesh size for the one-dimensional gap problem. The time integration was performed with the Explicit Euler method and approximately 2million time steps.

	Deviation w/ matrix type			
N_x	$(100, 0.1s)$	$(100, \infty)$	$(10, \infty)$	$(1, \infty)$
2^1	3.91×10^{-6}	3.98×10^{-6}	5.93×10^{-5}	9.30×10^{-5}
2^2	3.19×10^{-7}	3.21×10^{-7}	2.05×10^{-5}	1.06×10^{-4}
2^3	2.11×10^{-8}	2.12×10^{-8}	1.95×10^{-6}	5.20×10^{-5}
2^4	1.34×10^{-9}	1.35×10^{-9}	1.31×10^{-7}	5.96×10^{-6}
2^5	8.44×10^{-11}	8.45×10^{-11}	8.35×10^{-9}	5.46×10^{-7}
	Deviation w/ mesh size			
N_x	$(100, 0.1s)$	$(100, \infty)$	$(10, \infty)$	$(1, \infty)$
2^1	1.72×10^{-4}	3.44×10^{-4}	3.38×10^{-3}	2.80×10^{-2}
2^2	1.36×10^{-4}	2.73×10^{-4}	2.69×10^{-3}	2.43×10^{-2}
2^3	7.44×10^{-5}	1.49×10^{-4}	1.48×10^{-3}	1.40×10^{-2}
2^4	3.80×10^{-5}	7.61×10^{-5}	7.59×10^{-4}	7.38×10^{-3}

Table 1 is a summary of the numerical deviation between simulations. As we can see, the deviation with mesh size is order of magnitudes greater than the deviation caused by the change of matrix. In both cases, problems with slow diffusion (which present greater spatial gradients) present overall larger deviations with refinement - indicating that they need a relatively more refined mesh. These results indicate to us that the use of a lumped capacitance matrix is appropriate for the simulations.

3.2 Artificial porous media

The test case that we chose to showcase here is an artificial media with three pore sizes, all of them covering a similar area on the image. This medium is presented in the image below. It is a 200×200 pixel image with $1\mu m$ resolution and we consider a fluid with $\rho_1 = 5\mu m/s$, $\rho_2 = 10\mu m/s$, $D_0 = 2500\mu m^2/s$ and no bulk relaxation. The simulated domain is shown in Figure 5.

Figure 3 shows the decay simulated with the Dufort-Frankel method and 810^3 time steps and Figure 4 shows the ILT for the two signals. The time levels on the graph were the expected ones given by the surface-to-volume ratio of the pores, indicating good agreement.

The figure below shows the convergence of the numerical solution with the number of time steps. As we can see, an acceptable result ($\approx 0.1\%$ deviation) can be achieved by thousands of time steps fewer using the Dufort-Frankel instead of the Explicit Euler method - which has a severe limitation due to stability requirements.

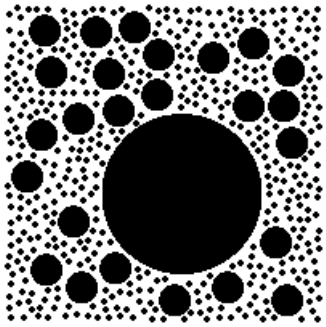

Figure 2. Artificial porous medium composed of three sizes of circular pore.

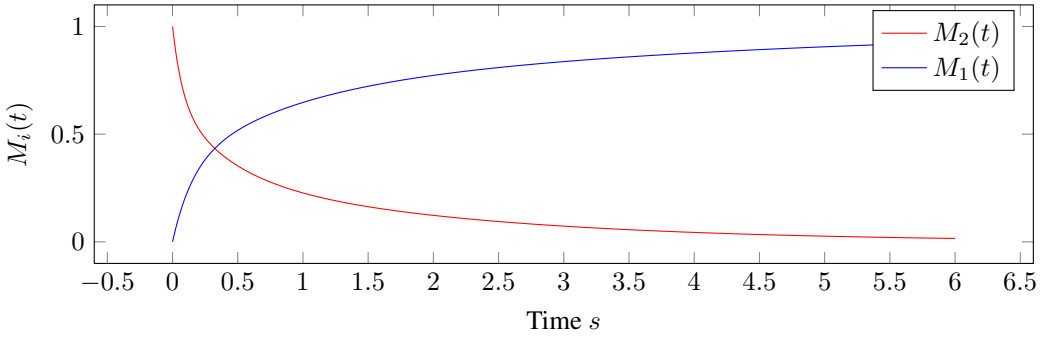

Figure 3. M_1 and M_2 decays for the artificial porous medium.

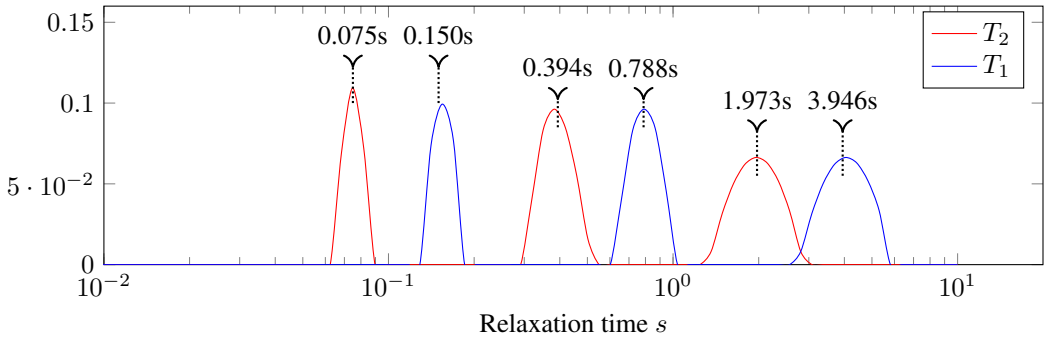

Figure 4. T_1 and T_2 distributions for the artificial porous medium. The time labels refer to the expected relaxation times calculated using the area and volume of the circular pores, in a fast diffusion scenario.

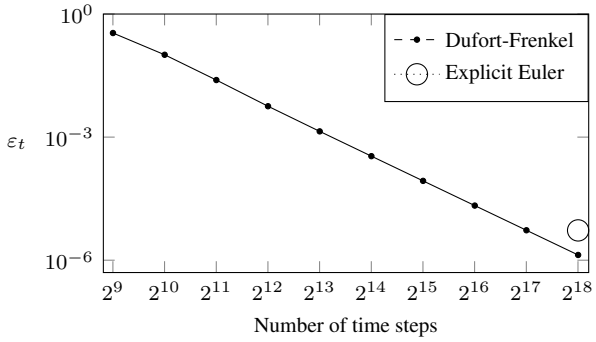

Figure 5. Numerical convergence with time-step size. The single Explicit Euler point is the beginning of stabillity.

4 Conclusion and future work

This work is part of an ongoing larger project, that aims to build massively parallel FEM implementations on GPU's to efficiently solve large image-based problems petrophysics problems.

This study shows that the use of a lumped mass system can solve the transient NMR problems efficiently without the need for either storing an additional matrix or the solution of linear systems in each time-step.

Additionally, hyperbolization methods like the Dufort-Frankel add a negligible amount of numerical error in exchange for unconditional stability. An the added error due to the hyperbolic effects diminishes with the reduction of the time step size, being negligible with time step sizes thousands of times smaller than the ones required by traditional explicit methods.

The next step in this study is to combine this fully explicit approach with a matrix-free methodology [7] to save memory in GPU implementations, and step towards 3D simulations.

Acknowledgements. This research was carried out in association with the ongoing RD project registered as ANP n^o 21289-4, "Desenvolvimento de modelos matemáticos, estatísticos e computacionais para o aperfeiçoamento da caracterização petrofísica de reservatórios por Ressonância Magnética Nuclear (RMN)" (UFF/Shell Brasil/ANP), sponsored by Shell Brasil under the ANP R&D levy as "Compromisso de Investimentos com Pesquisa e Desenvolvimento". The authors also recognize the support from CAPES, CNPq and FAPERJ .

Authorship statement. The authors hereby confirm that they are the sole liable persons responsible for the authorship of this work, and that all material that has been herein included as part of the present paper is either the property (and authorship) of the authors, or has the permission of the owners to be included here.

References

[1] L. Beltrachini, Z.A. Taylor, and A.F. Frangi. A parametric finite element solution of the generalised bloch–torrey equation for arbitrary domains. *Journal of Magnetic Resonance*, 259:126–134, 2015.

[2] L. Beltrachini, Z.A. Taylor, and A.F. Frangi. An efficient finite element solution of the generalised bloch-torrey equation for arbitrary domains. *Mathematics and Visualization*, none:3–14, 2016.

[3] G.R. Coates, L. Xiao, and M.G. Prammer. NMR logging: principles and applications. *Houston: Haliburton Energy Services*, 234, 1999.

[4] E.C. Du Fort and S.P. Frankel. Stability conditions in the numerical treatment of parabolic differential equations. *Mathematical Tables and Other Aids to Computation*, 7(43):135–152, 1953.

[5] K.J. Dunn, D.J. Bergman, and G.A. Latorraca Nuclear Magnetic Ressonance: Petrophysical and Logging Applications. *Handbook of geophysical exploration, Pergamon*, 2002.

[6] D. Galloway and D. Ivers. Slow-burning instabilitiesof dufort-frankel finite differencing. *The ANZIAM Journal*, 63(1):23–38, 2021.

[7] T. J. R. Hughes, I. Levit, and J. Winget. An element-by-element solution algorithm for problems of structural and solid mechanics. *Computer Methods in Applied Mechanics and Engineering*, 36(2):241-254, 1983

[8] O. Mohnke and N. Klitzsch. Microscale simulations of nmr relaxation in porous media considering internal field gradients. *Vadose Zone Journal*, 9:846, 04 2010.

[9] D. Nguyen, J.R. Li, D. Grebenkov, and D. Le Bihan. A finite elements method to solve the bloch–torrey equation applied to diffusion magnetic resonance imaging. *Journal of Computational Physics*, 263:283–302, 2014.

[10] V.D Nguyen, J. Jansson, J. Hoffman, and J.R. Li. A partition of unity finite element method for computational diffusion mri. *Journal of Computational Physics*, 375:271–290, 2018.

[11] S.D. Senturia and J.D. Robinson. Nuclear spin-lattice relaxation of liquids confined in porous solids. *Society of Petroleum Engineers Journal*, 10(03):237–244, 1970.